Inorganic Chemistry

Article

pubs.acs.org/IC

Copper(II) Complexes of Tetradentate Pyridyl Ligands Supported on Keggin Polyoxometalates: Single-Crystal to Single-Crystal Transformations Promoted by Reversible Dehydration Processes

Amaia Iturrospe, Beñat Artetxe, Santiago Reinoso, Leire San Felices, Pablo Vitoria, Luis Lezama, and Juan M. Gutiérrez-Zorrilla*

Departamento de Química Inorgánica, Facultad de Ciencia y Tecnología, Universidad del País Vasco UPV/EHU, P.O. Box 644, 48080 Bilbao, Spain

Supporting Information

ABSTRACT: Two new hybrid compounds constructed from Keggin type polyoxometalates and copper(II) complexes of tetradentate ligands containing amine and pyridyl groups, namely $[Cu(bpmen)(H_2O)][SiW_{12}O_{40}\{Cu(bpmen)\}]$ (**1**) and $[SiW_{12}O_{40}\{Cu(bpmpn)(H_2O)\}_2]\cdot 3H_2O$ (**2**) (bpmen, N,N′-dimethyl-N,N′-bis-(pyridin-2-ylmethyl)-1,2-diaminoethane; bpmpn, N,N′-dimethyl-N,N′-bis(pyridin-2-ylmethyl)-1,3-diaminopropane), have been synthesized under hydrothermal conditions and characterized by elemental analyses and infrared and Raman spectroscopy. Thermal stability of **1** and **2** has been studied by means of thermogravimetric analyses and variable temperature powder X-ray diffraction. Both compounds undergo single-crystal to single-crystal transformations promoted by reversible dehydration processes that have been followed by single-crystal X-ray diffraction. Structures of **1** and **2**, and also of their corresponding anhydrous phases **1a** and **2a**, have been established. The layered structure of **1** shows rows of monodecorated polyanions with complex cations occupying intralamellar spaces, whereas *trans*-didecorated species in **2** lead to stacked honeycomb-like metal−organic layers forming channels where Keggin clusters are accommodated. Structural differences relate to changes in the complex geometry and ligand conformation when going from bpmen to bpmpn. Dehydration of **1** promotes coordination of the complex countercation and consequent formation of a *cis*-didecorated species in **1a**, whereas changes in the structure of **2a** are more subtle. Structural variations upon dehydration are reflected in the electron paramagnetic resonance spectra.

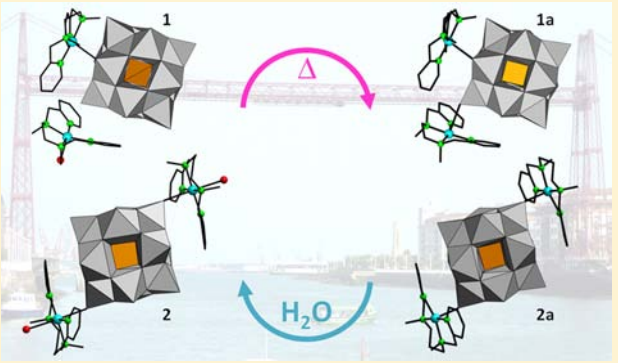

INTRODUCTION

Polyoxometalates (POMs) constitute a large family of transition-metal−oxide clusters. They have been widely recognized to exhibit remarkable compositional and structural diversity and properties that make them useful in different areas including catalysis, magnetism, materials science, and medicine.[1] A significant advance in the field of POM chemistry is the construction of hybrid compounds with transition-metal coordination complexes bearing organic ligands.[2] Functionalization of POMs allows for new properties and applications to be obtained because of the synergistic effect between the active inorganic and metal−organic building blocks. Such types of hybrids might bring POMs to a new area of advanced multifunctional materials.[3]

Copper(II) complexes represent exceptional moieties for the functionalization of POMs because of the geometrical flexibility of the Cu^{II} coordination sphere.[4] These complexes can add remarkable properties to the POM system because they play important roles in the active sites of cupro-proteins, as well as in the homogeneous catalysis for different organic reactions.[5] In the past years, our group reported several hybrid compounds based on Keggin type POMs and Cu^{II} complexes with simple, commercial bidentate ligands (acetate, oxalate, 2,2′-bipyridine, 1,10-phenanthroline).[6] Besides some magnetic aspects, we mainly focused our studies on the systematic analysis of the different intermolecular POM−ligand interactions governing the packing of such hybrids. In order to achieve further insight into the role played by these weak interactions, we decided to explore the structural influence of more elaborate organic ligands and selected tetradentate species containing amine and pyridil groups (N_2Py_2) for this purpose. Transition metal complexes with N_2Py_2 ligands have been successfully applied in catalytic and biological studies.[7] To our knowledge, the $[Mo_4O_{16}\{Cr(bispictn)\}_4](ClO_4)_4\cdot 3H_2O$ compound represents the only example where they have been combined with POM clusters.[8]

Received: November 20, 2012
Published: March 7, 2013

   dx.doi.org/10.1021/ic302499f | Inorg. Chem. 2013, 52, 3084−3093

Table 1. Crystallographic Data for Compounds 1 and 2 and Their Anhydrous Phases 1a and 2a

	1	1a	2	2a
formula	$C_{32}H_{46}Cu_2N_8O_{41}SiW_{12}$	$C_{32}H_{44}Cu_2N_8O_{40}SiW_{12}$	$C_{34}H_{58}Cu_2N_8O_{45}SiW_{12}$	$C_{34}H_{48}Cu_2N_8O_{40}SiW_{12}$
fw (g mol^{-1})	3559.99	3538.09	3660.11	3570.17
cryst syst	orthorhombic	orthorhombic	monoclinic	monoclinic
space group	*Pbca*	*Pbca*	$P2_1/n$	$P2_1/n$
T (K)	100(2)	423(2)	100(2)	423(2)
a (Å)	19.3953(6)	19.2671(3)	10.9853(2)	11.0092(7)
b (Å)	23.6891(7)	23.9764(4)	12.0992(3)	12.0532(7)
c (Å)	26.5521(10)	26.6345(5)	24.7010(6)	24.1712(17)
α (deg)	90	90	90	90
β (deg)	90	90	96.104(2)	98.403(6)
γ (deg)	90	90	90	90
V (Å^3)	12199.6(7)	12304.0(4)	3264.48(13)	3173.0(3)
Z	8	8	2	2
D_{calcd} (g cm^{-3})	3.875	3.820	3.713	3.737
μ (mm^{-1})	23.329	23.129	21.805	22.423
collected reflns	74996	84001	23034	22073
unique reflns (R_{int})	18587 (0.056)	13367 (0.046)	8067 (0.033)	6403 (0.048)
observed reflns [$I > 2\sigma(I)$]	12734	11442	6449	4964
params	577	573	320	293
$R(F)^a$ [$I > 2\sigma(I)$]	0.059	0.068	0.041	0.060
$wR(F^2)^a$ (all data)	0.112	0.133	0.085	0.203
GoF	1.091	1.310	1.098	1.071

$^a R(F) = \sum||F_o| - |F_c||/\sum|F_o|$. $wR(F^2) = \{\sum[w(F_o^2 - F_c^2)^2]/\sum[w(F_o^2)^2]\}^{1/2}$.

Here, we report the synthesis, spectroscopic characterization, and crystal structures of the first two hybrid compounds obtained from the interaction between POMs and Cu^{II}/N_2Py_2 complexes, namely, $[Cu(bpmen)(H_2O)][SiW_{12}O_{40}\{Cu(bpmen)\}]$ (**1**, bpmen: N,N′-dimethyl-N,N′-bis-(pyridin-2-ylmethyl)-1,2-diaminoethane) and $[SiW_{12}O_{40}\{Cu(bpmpn)(H_2O)\}_2]\cdot 3H_2O$ (**2**, bpmpn: N,N′-dimethyl-N,N′-bis(pyridin-2-ylmethyl)-1,3-diaminopropane). Both compounds undergo single-crystal to single-crystal transformations promoted by reversible dehydration processes. The structures of the anhydrous phases $[SiW_{12}O_{40}\{Cu(bpmen)\}_2]$ (**1a**) and $[SiW_{12}O_{40}\{Cu(bpmpn)\}_2]$ (**2a**) have also been determined by single-crystal X-ray diffraction, and structural modifications upon dehydration have been detected by electron paramagnetic resonance spectroscopy.

EXPERIMENTAL SECTION

Materials and Methods. The $K_8[\alpha\text{-}SiW_{11}O_{39}]\cdot 13H_2O$ POM precursor was synthesized as described in the literature and identified by infrared spectroscopy.[9] All other chemicals were obtained from commercial sources and used without further purification. Carbon, hydrogen, and nitrogen were determined on a Perkin-Elmer 2400 CHN analyzer. ^{1}H Nuclear Magnetic Resonance (NMR) spectra of the ligands (Figure S1 in the Supporting Information) were recorded on a Bruker AC-300 spectrometer. Infrared (IR) spectra were obtained as KBr pellets on a SHIMADZU FTIR-8400S spectrometer. Raman spectra were recorded on single crystals by using a Renishaw InVia Raman spectrometer, joined to a Leica DMLM microscope with a Leica 50 × N Plan objective and excitation wavelength of 514 nm (Modu-Laser). Thermogravimetric and Differential Thermal Analyses (TGA/DTA) were carried out from room temperature to 750 °C at a rate of 5 °C min^{-1} on a TA Instruments 2960 SDT thermobalance under a 100 cm^3·min^{-1} flow of synthetic air. Electron Paramagnetic Resonance (EPR) spectra were recorded on Bruker ELEXSYS 500 (superhigh-Q resonator ER-4123-SHQ) and Bruker EMX (ER-510-QT resonator) continuous wave spectrometers for Q- and X-bands, respectively (magnetic calibration: NMR probe; frequency inside the cavity determined with microwave counter).

Synthesis of bpmen and bpmpn Ligands. Bpmen and bpmpn ligands were synthesized following the literature procedure for bpmen with slight modifications.[10]

N,N′-Dimethyl-N,N′-bis-(pyridin-2-ylmethyl)-1,2-diaminoethane (bpmen). To a solution of 2-(chloromethyl)-pyridine hydrochloride (3.0 g, 18.3 mmol) in water (10 mL) was dropwise added a solution of K_2CO_3 (5.1 g, 37 mmol) in water (15 mL). After stirring at room temperature for 30 min, the reaction mixture was extracted with CH_2Cl_2 (3 × 20 mL). The organic layers were combined, dried over Na_2SO_4, and concentrated in vacuo to afford an orange oil. This free-base product (2.2 g, 17.5 mmol) was dissolved in CH_2Cl_2 (10 mL) and dropwise added to N,N′-dimethylethylenediamine (0.942 mL, 8.75 mmol) dissolved in CH_2Cl_2 (25 mL). After the slow addition of aqueous 1 M NaOH (20 mL, 20 mmol), the resulting mixture was stirred for 60 h at room temperature, followed by the rapid addition of a second fraction of aqueous 1 M NaOH (20 mL, 20 mmol). The aqueous layer was then extracted with CH_2Cl_2 (3 × 50 mL), and the combined organic layers were dried over Na_2SO_4 to afford the bpmen ligand as an orange oil after concentration in vacuo (1.8 g, yield: 76%). ^{1}H NMR (300 MHz, CD_3OD): δ 2.20 (s, 6H, −N−CH_3), 2.57 (s, 4H, −CH_2−CH_2−), 3.61 (s, 4H, N−CH_2−Py), 7.04−8.46 (m, 8H, Py ring) ppm.

N,N′-Dimethyl-N,N′-bis(pyridin-2-ylmethyl)-1,3-diaminopropane (bpmpn). The above procedure was followed but using N,N′-dimethyl-1,3-propanediamine (1.094 mL, 8.75 mmol) instead of N,N′-dimethylethylenediamine. The bpmpn ligand was isolated as an orange oil (2.0 g, yield: 81%). ^{1}H NMR (300 MHz, CD_3OD): δ 1.73 (m, 2H, −CH_2−(CH_2N)$_2$), 2.21 (s, 6H, −N−CH_3), 2.45 (t, 4H, −CH_2N−), 3.61 (s, 4H, Py−CH_2−N−), 7.08−8.50 (m, 8H, Py ring) ppm.

Synthesis of Compounds 1 and 2. *$[Cu(bpmen)(H_2O)][SiW_{12}O_{40}\{Cu(bpmen)\}]$ (1).* A mixture of $K_8[\alpha\text{-}SiW_{11}O_{39}]\cdot 13H_2O$ (0.322 g, 0.1 mmol), $Cu(CH_3COO)_2$ (0.036 g, 0.3 mmol), bpmen (0.054 g, 0.2 mmol), and 1 M KCH_3COO/CH_3COOH buffer (25 mL) was stirred for 1 h, transferred to a 50 mL Teflon-lined autoclave, and kept at 140 °C for 3 days. After slowly cooling to room temperature for 48 h, blue plates of **1** suitable for single-crystal X-ray diffraction were obtained (90 mg, yield: 25%, based on W). Anal. Calcd (found) for $C_{32}H_{46}Cu_2N_8O_{41}SiW_{12}$: C, 10.80 (10.45); H, 1.30 (1.56); N, 3.15 (3.08). IR (cm^{-1}, KBr pellet): 3086(w), 2924(w),

dx.doi.org/10.1021/ic302499f | Inorg. Chem. 2013, 52, 3084−3093

1613(m), 1450(m), 1304(w), 1258(w), 1018 (m), 964(s), 918(vs), 880(s), 802(vs), 756(sh), 525(m), 478(w). Raman (cm^{-1}, single crystal): 3062(w), 2930(w), 1614(m), 1554(m), 1460(m), 1305(w), 1140(w), 1047(w), 1025(w), 985(s), 956(m), 885(m), 550(w), 517(w), 225(w), 211(w), 148(w), 142(w).

*[[$SiW_{12}O_{40}${Cu(bpmpn)(H_2O)}$_2$]·3H_2O (**2**).* The synthetic conditions were similar to those of **1**, but bpmpn (0.057 g, 0.2 mmol) was used instead of bpmen. A mixture of an orange polycrystalline powder and orange plates of **2** suitable for single-crystal X-ray diffraction was isolated (75 mg, yield: 20% based on W). Crystals were manually separated for structure determination. Powder X-ray diffraction shows that the polycrystalline fraction is also compound **2** (Figure S2 in the Supporting Information). Anal. Calcd (found) for $C_{34}H_{58}Cu_2N_8O_{45}SiW_{12}$: C, 11.16 (11.75); H, 1.59 (1.53); N, 3.06 (2.96). IR (cm^{-1}, KBr pellet): 3117(w), 2924(w), 1612(m), 1474(m), 1443(m), 1296(w), 1258(w), 1011(m), 964(s), 918(vs), 880 (s), 795(vs), 532(m), 478(w). Raman (cm^{-1}, single crystal): 3064(w), 2937(w), 1614(m), 1561(m), 1311(w), 1141(w), 1044(w), 1014(w), 987(s), 954(m), 890(m), 540(w), 517(w), 227(w), 209(w), 143(w).

X-Ray Crystallography. Crystal data for **1** and **2** and their anhydrous phases **1a** and **2a** are given in Table 1. Data for **1** and **2** were collected at 100(2) K on an Oxford Diffraction Xcalibur diffractometer (graphite monochromated Mo Kα radiation, λ = 0.71073 Å, Sapphire CCD detector). In the case of **1a** and **2a**, data were collected at 423(2) K on an Agilent Technologies SuperNova diffractometer (mirror-monochromated Mo Kα radiation, λ = 0.71073 Å, Eos CCD detector) equipped with an Oxford Cryostream 700 PLUS temperature device. In all cases, data frames were processed (unit cell determination, intensity data integration, correction for Lorentz and polarization effects, and analytical absorption correction) using the CrysAlis software package.[11] The structures were solved using OLEX[12] and refined by full-matrix least-squares with SHELXL-97.[13] Final geometrical calculations were carried out with Mercury[14] and PLATON[15] as integrated in WinGX.[16] Thermal vibrations were treated anisotropically for heavy atoms (W, Cu, Si). Hydrogen atoms of the organic ligands were placed in calculated positions and refined using a riding model with standard SHELXL parameters. The bridging O atoms of the Keggin clusters were disordered in two positions each, the occupancies being 40/60 for **1**, 30/70 for **1a**, 50/50 for **2**, and 45/55 for **2a**.

Powder X-ray diffraction (PXRD) data were collected on a Bruker D8 Advance diffractometer operating at 30 kV and 20 mA and equipped with a Cu tube (λ = 1.5418 Å), a Vantec-1 PSD detector, and an Anton Parr HTK2000 high-temperature furnace. The powder patterns were recorded in 2θ steps of 0.033° in the 5 ≤ 2θ ≤ 39 range, counting for 0.3 s per step using a Pt sample holder. Data sets were recorded from 30 to 890 °C every 20 °C, with a 0.16 °C s^{-1} heating rate between temperatures.

RESULTS AND DISCUSSION

Synthesis. The bpmen ligand was synthesized following the reported method but with a slight modification in the final purification step.[10] This route was also used to prepare bpmpn but employing N,N′-dimethyl-1,3-propane-diamine instead of N,N′-dimethyl-ethylenediamine (Figure S3 in the Supporting Information). Compounds **1** and **2** were obtained by treating a mixture of $K_8[\alpha\text{-}SiW_{11}O_{39}]$, $Cu(CH_3COO)_2$, and N_2Py_2 ligands (1:3:2 ratio) in a potassium acetate buffer solution under hydrothermal conditions.

Since **1** and **2** contain the plenary $[\alpha\text{-}SiW_{12}O_{40}]^{4-}$ anion instead of the monolacunary $[\alpha\text{-}SiW_{11}O_{39}]^{8-}$ precursor, we tried to prepare both compounds under the same conditions, but using $K_4[\alpha\text{-}SiW_{12}O_{40}]$ synthesized as reported.[9] Reactions were carried out with both the original 1:3:2 and the stoichiometric 1:2:2 ratios, resulting in greenish blue (bpmen) and brown (bpmpn) precipitates. Although containing $[\alpha\text{-}SiW_{12}O_{40}]^{4-}$ clusters and N_2Py_2 ligands according to IR spectroscopy, none of these precipitates correspond to pure **1** and **2** as shown by PXRD analyses (Figure S2 in the Supporting Information). Isolation of these types of compounds also depends on the choice of the transition metal. We could not obtain analogues of **1** and **2** under the same conditions when Cu^{II} was substituted by Co^{II} or Ni^{II} but only amorphous precipitates that could not be characterized adequately. The flexible coordination geometries that Cu^{II} can adopt due to the Jahn−Teller effect seem to play a key role in the formation of **1** and **2**.

IR and Raman Spectroscopy. IR spectra of **1** and **2** are differentiated in metal−organic and inorganic regions above and below 1000 cm^{-1}, respectively (Figure S4 in the Supporting Information). The characteristic bands of the $[\alpha\text{-}SiW_{12}O_{40}]^{4-}$ Keggin cluster can be clearly identified in the inorganic region,[17] their positions being in agreement with those calculated by DFT.[18] The metal−organic region is dominated by signals of medium intensity appearing in the 1440−1615 cm^{-1} range and associated to C═C and C═N stretching vibrations. Compound **1** shows a single peak at 1450 cm^{-1}, whereas splitting of this signal is observed for **2**. The group of overlapped peaks centered at 2925 cm^{-1} and the weak resonances at ∼1260 and 1300 cm^{-1} originate from aliphatic C−H bonds, whereas the multiplet above 3000 cm^{-1} is indicative of aromatic C−H bonds. IR spectroscopy allows for determining the metal−organic grafting on the POM surface because such coordination produces red shifting of the bands associated to W−O_t bonds compared to those of the naked Keggin anion. This mainly affects to the peak originating from the ν_{as}(W−O_t) mode, with displacements of ca. 15 cm^{-1}.

Raman spectra of **1** and **2** (Figure S5 in the Supporting Information) are dominated by a pair of narrow peaks in the 950−990 cm^{-1} range that are characteristic of the ν_{as}(W−O_t) vibration of $[SiW_{12}O_{40}]^{4-}$.[17] They also exhibit additional signals evidencing the presence of N_2Py_2 ligands: two broad bands at 3060−3065 and 2930−2940 cm^{-1} related to aromatic and aliphatic C−H bonds and a group of peaks between 1000 and 1675 cm^{-1} originating from C═C/C═N stretching and C−H bending.

Thermal Analyses. Thermal stability for **1** and **2** was investigated by TGA/DTA and variable temperature PXRD. For both compounds, thermal decomposition proceeds via three steps with very similar profiles (Figures 1a and S6 in the Supporting Information). The initial endothermic mass loss below ∼160 °C for **1** and 145 °C for **2** corresponds to dehydration and implies the release of one water molecule for the former (calcd 0.5%; found 0.7%) and five water molecules for the latter (calcd 2.5%; found 2.2%). The resulting anhydrous phases **1a** and **2a** are thermally stable up to ∼290 and 255 °C, respectively. These thermal stability ranges are followed by two overlapped exothermic mass losses corresponding to organic pyrolysis and decomposition of the POM framework. The overall mass loss is in good agreement with two bpmen ligands in **1** (calcd 15.2%; found 15.3%) and two bpmpn ligands in **2** (calcd 15.7%; found 16.0%). Final residues are obtained above 630 °C for both **1** (calcd 84.3%; found 83.6%) and **2** (calcd 82.0%; found 81.4%)

PXRD experiments between room temperature and 890 °C (Figure 1b) show that **1** and **2** retain crystallinity upon dehydration. No substantial variations in the positions and intensities of the diffraction maxima of the resulting anhydrous phases **1a** and **2a** are observed compared to those of the initial compounds, indicating that dehydration does not result in

dx.doi.org/10.1021/ic302499f | Inorg. Chem. 2013, 52, 3084−3093

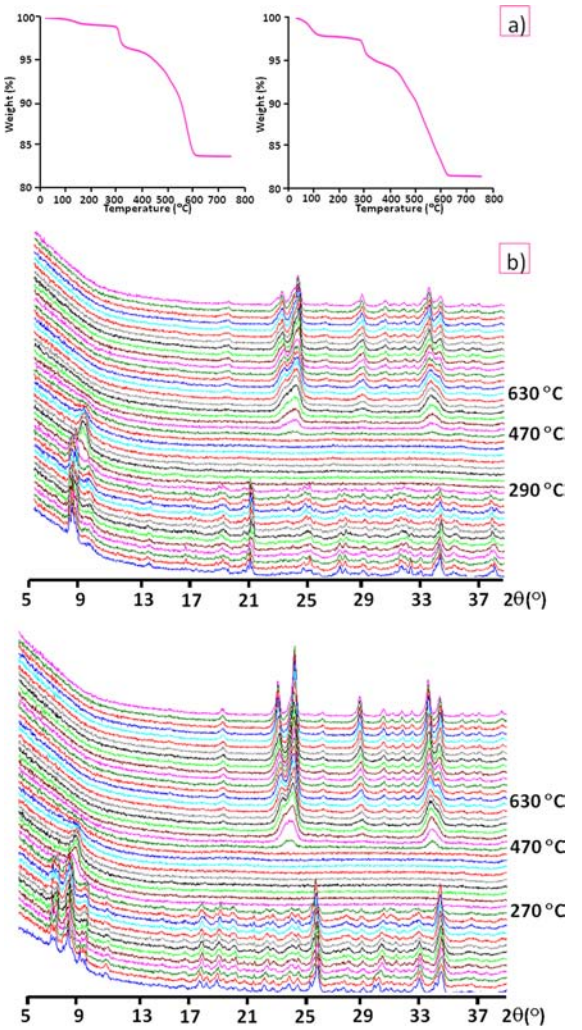

Figure 1. (a) TGA curves of **1** (left) and **2** (right). (b) Variable temperature powder X-ray diffractograms of **1** (top) and **2** (bottom).

drastic modifications of the cell parameters. The crystalline anhydrous phases are stable up to 290 °C for **1a** and 270 °C for **2a** in agreement with the above observations on the TGA curves. Both transform into amorphous solids in the temperature range corresponding to the ligand pyrolisis. New crystalline phases start appearing at temperatures above 470 °C and they reach complete formation at 630 °C, which corresponds to the end of the third TGA mass losses. These final residues were both identified as mixtures of monoclinic WO_3 (PDF 88−269)[19] and triclinic $CuWO_4$ (PDF 43−1035)[20] with Scheelite-type structure (Figure S7 in the Supporting Information). This fact is fully consistent with our previous observations in related systems.[6g]

Single-Crystal X-ray Diffraction Studies. Encouraged by the TGA/DTA and PXRD results over polycrystalline samples, we decided to carry out similar studies by single-crystal X-ray diffraction. Single crystals of **1** and **2** for which complete structural measurements were previously performed at 100(2) K were selected. The temperature was raised from room temperature to 215 °C at a rate of 1 °C min^{-1}.

Both crystals preserved their integrity and crystallinity in the complete temperature range, allowing for complete unit cell determinations being performed at room temperature, 60, 105, 150, 185 and 215(2) °C (Table 2). Noticeable shortening of the *a* parameter for **1** and the *c* parameter for **2** with consequent contraction of the unit cell volumes is observed when going from 105 to 150 °C (Figure 2). These variations

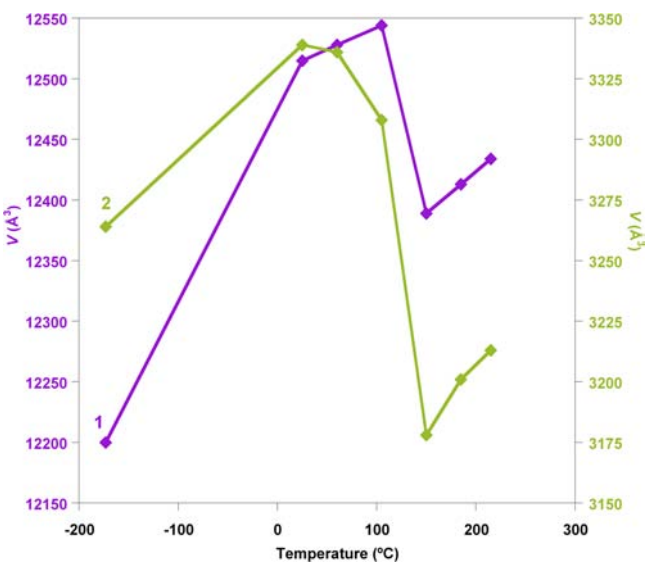

Figure 2. Thermal variation of the unit cell volumes of **1** and **2**.

Table 2. Unit Cell Parameters of 1 and 2 at Different Temperatures

T (°C)	*a* (Å)	*b* (Å)	*c* (Å)	*α* (deg)	*β* (deg)	*γ* (deg)	*V* (Å³)
			compound 1				
r.t.	19.547(2)	23.914(4)	26.773(3)	90	90	90	12515(3)
60	19.552(2)	23.925(3)	26.778(3)	90	90	90	12528(3)
105	19.562(3)	23.958(5)	26.766(5)	90	90	90	12544(4)
150	19.333(2)	23.995(4)	26.707(3)	90	90	90	12389(3)
185	19.321(2)	24.051(4)	26.712(3)	90	90	90	12413(3)
215	19.325(2)	24.074(4)	26.727(3)	90	90	90	12434(3)
			compound 2				
r.t.	11.0914(17)	12.2144(16)	24.805(4)	90	96.450(17)	90	3339(1)
60	11.088(4)	12.222(4)	24.785(11)	90	96.68(5)	90	3336(2)
105	11.046(3)	12.155(3)	24.785(8)	90	96.15(3)	90	3308(2)
150	11.012(2)	12.059(3)	24.202(7)	90	98.55(3)	90	3178(2)
185	11.044(4)	12.084(4)	24.242(9)	90	98.40(4)	90	3201(2)
215	11.067(4)	12.105(4)	24.248(9)	90	98.43(4)	90	3213(2)

dx.doi.org/10.1021/ic302499f | *Inorg. Chem.* 2013, 52, 3084−3093

indicate formation of the corresponding anhydrous phases **1a** and **2a** in good agreement with TGA results. Thus, full data collections for both crystals were performed at 423(2) K and the structures of **1a** and **2a** were determined. These showed not only the expected complete loss of water molecules, but also other significant structural changes that will be commented in detail below.

After cooling down the single crystals of both compounds to room temperature, they were kept under a wet atmosphere for approximately one month, and intensity data were collected at 100(2) K. The unit cells of the initial, hydrated **1** and **2** were again obtained, and although collections were of poorer quality because of partial cracking of the crystals during rehydration, they diffracted acceptably enough for performing preliminary structural solutions. X-ray crystallographic data in CIF format for rehydrated **1** are provided in the Supporting Information. In the case of rehydrated **2**, the Keggin subunit and the CuN_4O_2 chromophore including the axial aquo ligand were located, but unfortunately, the quality of the data did not allow complete determination of the bpmpn ligand. These observations demonstrate that both **1** and **2** undergo single-crystal to single-crystal transformations at high temperatures promoted by the previously described dehydration processes. Moreover, these transformations implying substantial structural modifications beyond the loss of the coordination/hydration water molecules are completely reversible upon rehydration with retention of the crystallinity.

All four compounds contain discrete, hybrid species formed by $[SiW_{12}O_{40}]^{4-}$ clusters onto which Cu^{II}/N_2Py_2 complexes are grafted. In all cases, the $[SiW_{12}O_{40}]^{4-}$ anion shows the characteristic structure of the α-Keggin isomer consisting of a central SiO_4 tetrahedron surrounded by four vertex-sharing W_3O_{13} trimers, each composed of three edge-sharing WO_6 octahedra. Bond lengths and angles compare well with the DFT-optimized ones[18b] (Table S1 in the Supporting Information).

Cu^{II}/bpmen and Cu^{II}/bpmpn Complexes. There are two different Cu^{II}/bpmen complexes in the crystal structure of **1**: one supported {Cu(bpmen)} metal–organic block (Cu1A) and one $[Cu(bpmen)(H_2O)]^{2+}$ complex acting as a counter-cation (Cu1B). In both cases, the coordination geometry of the Cu^{II} centers may be considered as tetragonally elongated square-pyramidal with four N atoms in the basal plane and the apical position occupied by one terminal O atom from the $[SiW_{12}O_{40}]^{4-}$ cluster for Cu1A and one water molecule for Cu1B (Figure 3, top). Coordination geometry and bond lengths (Table 3) and angles (Table S2 in the Supporting Information) are consistent with the scarce Cu^{II}/bpmen complexes that have been structurally characterized to date.[21] The sixth position is in both cases blocked by a terminal O atom of a contiguous POM at $Cu\cdots O_{POM}$ distances slightly above 3.0 Å.

When **1** is heated to 150 °C, a loss of the water molecule coordinated to Cu1B takes place, in such a way that the complex cation shifts and coordinates to the O_{POM} atom that was blocking its sixth position. The square-pyramidal geometry in this fragment is thereby maintained but with switching of the apical coordination position and significant lengthening of the $Cu-O_{ap}$ bond. In contrast, the $Cu\cdots O_{POM}$ distance to the O atom blocking the sixth position of Cu1A is shortened by less than 0.1 Å upon dehydration, resulting in the strengthening of the interaction between adjacent hybrid POMs. If this long-range contact is considered as semicoordination, the square-pyramidal geometry of Cu1A should be then described as elongated octahedral (Figure 3, bottom).

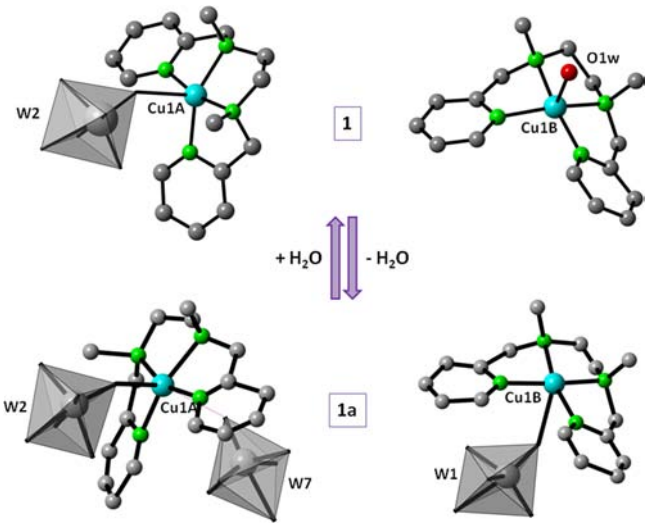

Figure 3. The {Cu(bpmen)} metal–organic block and the $[Cu(bpmen)(H_2O)]^{2+}$ cation in **1** (top) compared to the corresponding complexes in the anhydrous **1a** (bottom).

In contrast to **1**, compound **2** contains only one type of Cu^{II}/bpmpn complex grafted at the POM. The Cu atom shows elongated octahedral coordination geometry with four N atoms in the equatorial plane and one water molecule and one terminal O atom of the Keggin anion in axial positions (Figure 4, left). Selected bond lengths are shown in Table 3, and they are consistent with those reported for $[Cu(bpmpn)](ClO_4)_2$[21d] and $[Cu(NCS)(bpmpn)](ClO_4)$.[22] When **2** is heated to 150 °C, the axial water molecule is released and the octahedral geometry of the Cu atom becomes square-pyramidal (Figure 4, right).

There are two possible isomers for this type of Cu^{II}/N_2Py_2 complex: *cis* when the CH_3 groups on the amine N atoms (NCH_3) are on the same side of the CuN_4 equatorial/basal plane and *trans* when they point to opposite directions (Figure S8 in the Supporting Information). According to DFT calculations,[21d] the *cis* isomer is favored for Cu^{II}/bpmen complexes thanks to intramolecular hydrogen bonding between the two NCH_3 groups and the O atom occupying the apical position, resulting in the stabilization of the square-pyramidal geometry. This is exactly what we observed for both the {Cu(bpmen)} metal–organic block and the $[Cu(bpmen)(H_2O)]^{2+}$ cation in **1** (Figure 3). The *cis* form is maintained for both complexes in the anhydrous **1a** despite the fact that coordination of the latter to the Keggin cluster upon dehydration results in methyl substituents and apical O_{POM} pointing to opposite directions and the consequent impossibility of intramolecular hydrogen bonding.

In contrast to Cu^{II}/bpmen complexes, the *trans* isomer with the chair conformation is favored for the Cu^{II}/bpmpn fragments. As shown by DFT calculations, there is no hydrogen bonding between NCH_3 groups and apical O atoms, but the larger chelating ring around the Cu^{II} center facilitates accommodation of two O atoms in axial positions, in such a way that octahedral geometries are stabilized. Again, this is the situation observed for the {Cu(bpmpn)} metal–organic block in **2** (Figure 4). However, this complex undergoes *trans* to *cis* isomerization with boat conformation upon dehydration. Although DFT calculations indicate that stabilization of the

dx.doi.org/10.1021/ic302499f | *Inorg. Chem.* 2013, 52, 3084–3093

Table 3. Selected Bond Lengths (Å) for the Cu^{II}/bpmen and Cu^{II}/bpmpn Complexes

Cu^{II}/bpmen complexes						Cu^{II}/bpmpn complexes		
Cu1A			Cu1B			Cu1		
	1	1a		1	1a		2	2a
Cu1A–N1A	2.001(11)	2.04(2)	Cu1B–N1B	1.993(12)	1.98(2)	Cu1–N1	2.011(9)	2.051(19)
Cu1A–N2A	2.022(13)	2.14(3)	Cu1B–N2B	2.019(11)	2.01(2)	Cu1–N2	2.025(8)	2.05(2)
Cu1A–N3A	2.015(12)	1.95(3)	Cu1B–N3B	2.041(12)	2.02(3)	Cu1–N3	2.030(9)	2.01(3)
Cu1A–N4A	1.996(11)	2.008(19)	Cu1B–N4B	1.998(11)	1.984(18)	Cu1–N4	1.979(8)	2.03(2)
Cu1A–O2A	2.357(9)	2.436(16)	Cu1B–O1W	2.242(10)		Cu1–O1	2.610(7)	2.333(18)
Cu1A···O7A	3.057(10)	2.985(17)	Cu1B···O1A	3.089(12)	2.752(18)	Cu1–O1w	2.789(11)	

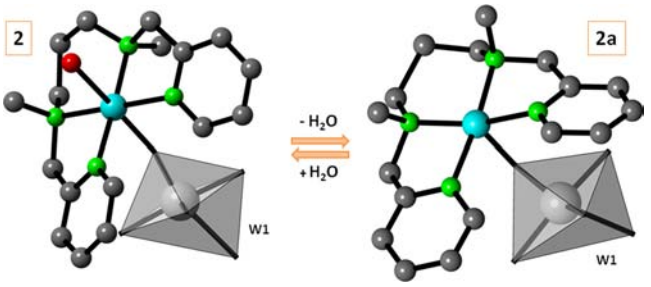

Figure 4. The {Cu(bpmpn)(H_2O)} metal–organic block in **2** (left) and its anhydrous form in **2a** (right).

cis isomer for Cu^{II}/bpmpn complexes is not favored, the high temperatures and the absence of a nearby donor atom for potential hexa-coordination induce this form to be present in the anhydrous **2a**.

Crystal Packing of Compounds 1 and 1a. Compound **1** contains the $[SiW_{12}O_{40}\{Cu(bpmen)\}]^{2-}$ discrete POM composed of one {Cu(bpmen)} metal–organic block supported on a Keggin cluster via axial coordination to a terminal O atom (Figure 5, top). The crystal packing can be viewed as corrugated hybrid layers stacked along the *c* axis where the POMs form rows along the [010] direction (Figure 6). The N4A pyridyl ring is sandwiched between tetrameric $\{W_4O_{18}\}$ faces of two contiguous polyanions in a row, whereas the N1A ring is placed over a $\{W_3O_{13}\}$ trimer of an adjacent POM. The distances of the ring centroids to the average planes of the tetramers/trimers defined by their bridging and terminal O atoms (Figure S9 in the Supporting Information) are comparable to those found in related hybrid POMs with dimeric Cu^{II}/ac/phen metal–organic blocks[6e] or in the diazine salts of the $[PMo_{12}O_{40}]^{3-}$ anion,[23] for which the existence of aromatic interactions with POM surfaces have been demonstrated on the basis of *ab initio* or Hirschfeld surface calculations. The $[Cu(bpmen)(H_2O)]^{2+}$ counterions are located in intralamellar spaces reinforcing the POM association. The apical water molecules link contiguous POMs in a row via strong hydrogen bonding with terminal O atoms ($O_{ap}\cdots O_{POM}$ = 2.951(16), 2.724(15) Å), whereas an extended network of C–H···O_{POM} interactions connects adjacent rows (Table S3 in the Supporting Information).

Dehydration of **1** results in **1a** with considerable variations in the crystal structure. Loss of the apical water molecule in the coordination sphere of Cu1B and consequent coordination to the O_{POM} atom which was blocking its sixth position leads to formation of the neutral $[SiW_{12}O_{40}\{Cu(bpmen)\}_2]$ hybrid species showing two metal–organic blocks supported on two edge-shared WO_6 octahedra in relative *cis* arrangement (Figure 5, bottom). Displacement of the Cu1B complexes leads to

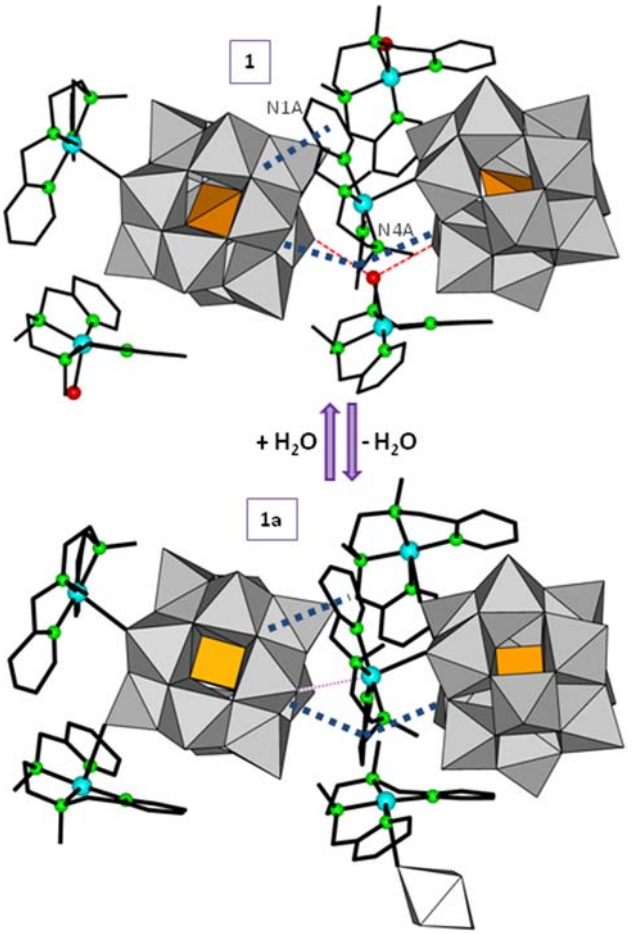

Figure 5. Top: Two adjacent $[SiW_{12}O_{40}\{Cu(bpmen)\}]^{2-}$ POMs and their associated $[Cu(bpmen)](H_2O)]^{2+}$ cations in **1** (O_{ap}–H···O_{POM} hydrogen bonds, red dashed lines; POM–aromatic interactions, blue dotted lines). Bottom: Newly formed $[SiW_{12}O_{40}\{Cu(bpmen)\}_2]$ neutral species in **1a**, showing the structural modifications promoted by dehydration (long-range Cu···O_{POM} contact: lilac dotted line).

contraction of the structure in the [100] direction. This is reflected in a closer packing of the POM rows in the layers and consequent shortening of the *a* cell parameter. The association between adjacent POMs balances the loss of the O_{ap}–H···O_{POM} interactions with the strengthening of the remaining intermolecular contacts, in such a way that while the distance of the N1A ring to the W_3O_{13} trimer is shortened, Cu1A undergoes slight displacement toward the O_{POM} atom blocking its sixth coordination position (Figure 6, bottom).

Crystal Packing of Compounds 2 and 2a. In contrast to the hybrid polyanion in **1**, the neutral species of **2** with C_i symmetry shows two supported {Cu(bpmpn)(H_2O)} metal–

dx.doi.org/10.1021/ic302499f | Inorg. Chem. 2013, 52, 3084–3093

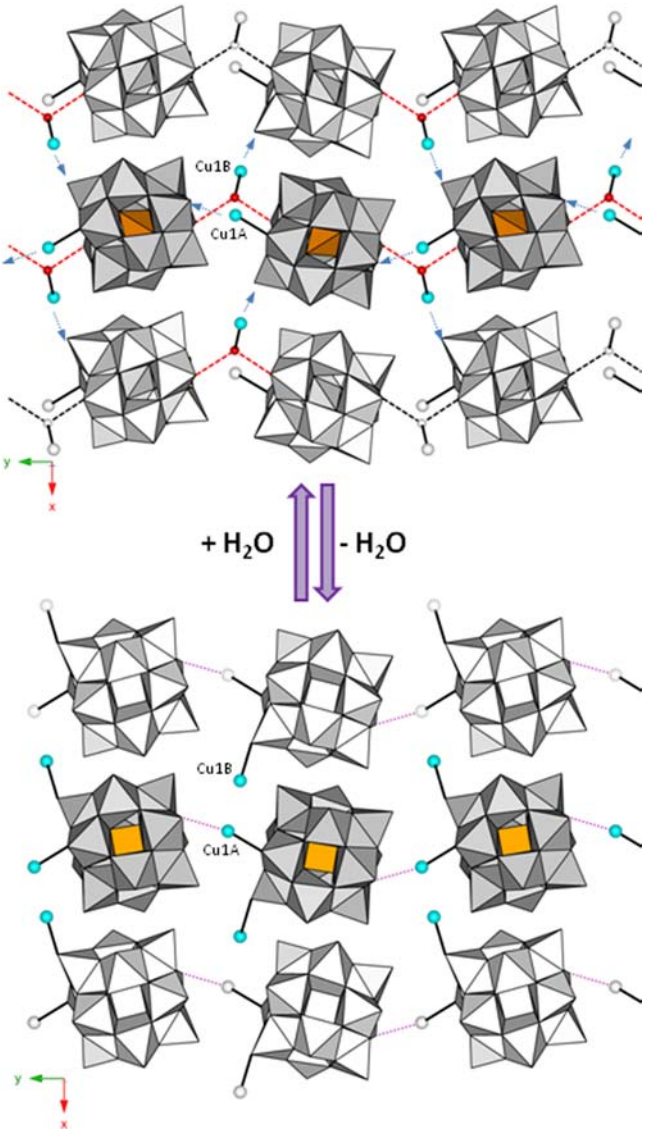

Figure 6. Comparison between the hybrid layers in **1** (top) and its anhydrous form **1a** (bottom) highlighting the structural transformation promoted by dehydration in the colored central row (color code same as Figure 5; bpmen ligands omitted for clarity).

organic blocks in relative *trans* arrangement via axial coordination to terminal O atoms. The complexes are anchored in such a way that intramolecular $\{W_4O_{18}\}$–aromatic interactions involving one of the pyridyl rings are established (Figure 7, top).

The additional methylene unit in the N–$(CH_2)_n$–N bridge with associated change in the ligand conformation and complex geometry results not only in a different hybrid species in **2** but also in a different type of crystal packing. This can be described as honeycomb-like metal–organic layers parallel to the (10−1) plane where an intricate network of C–H···O_w and O_w···O_w interactions involving methyl groups and pyridyl rings and coordination/hydration water molecules link the {Cu(bpmpn)-(H_2O)} fragments (Figure 8, top). The fragments form strings along the [010] direction via hydrogen contacts involving NCH_3 groups and aquo ligands, whereas hydration water molecules connect adjacent strings. Stacking of metal–organic layers generates hexagonal channels running parallel to the *a* axis where rows of Keggin clusters are accommodated (Figure

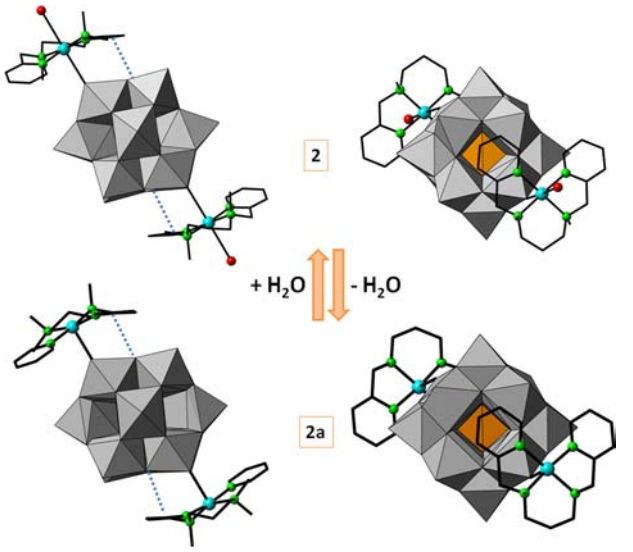

Figure 7. The $[SiW_{12}O_{40}\{Cu(bpmpn)(H_2O)_2\}_2]$ species in **2** (top) and its anhydrous form **2a** (bottom). Intramolecular POM–aromatic interaction represented as blue dotted lines.

8, bottom). The Keggin subunits occupy interlamellar spaces surrounded by six complexes for each metal–organic layer, and they are hydrogen bonded by hydration water molecules forming intercalated inorganic layers (Figure S10 in the Supporting Information).

The crystal packing of **2** does not undergo drastic changes upon dehydration as for **1**. The architecture of the hybrid species in the anhydrous phase **2a** is preserved but for the change in the complex geometry commented above (Figure 7, bottom). The arrangement of six complexes around a central Keggin cluster is also maintained in the metal–organic layers despite the fact that release of the water molecules destroys the C–H···O_w network (Figure S11 in the Supporting Information). However, there is a compression of the structure that is basically reflected in a significant shortening of the *c* cell parameter. This compression arises from a closer packing of the $[SiW_{12}O_{40}]^{4-}$ rows upon release of the interstitial hydration water molecules, which is accompanied by an overall contraction of the hexagonal-like metal–organic motifs, as indicated by shortening of most of the Cu···Cu distances (Figures S10 and S11 in the Supporting Information). Moreover, the *trans*-to-*cis* ligand isomerization generates additional sets of C_{NCH3}–H···O_{POM} contacts (Table S4 in the Supporting Information), so that reinforcement of these interactions seems to play a key role in stabilizing the crystal packing in absence of the C–H···O_w network.

EPR Spectroscopy. Although **1** displays two independent Cu^{II} centers, the Q-band spectrum is characteristic of an isolated Cu^{II} chromophore with axial **g** tensor and four-line hyperfine splitting on the parallel region originating from a spin doublet $S = 1/2$ interacting with a single $I = 3/2$ nucleus (Figure 9, top). However, simulation of the spectrum with axial symmetry did not result in a completely satisfactory fit. This fact is probably due to overlapping of two individual signals corresponding to the coexisting Cu1A and Cu1B centers with virtually identical coordination geometries. These signals must be very similar in the parallel region, and the average of the calculated $g_{\|}$ and $A_{\|}$ values (2.223 and 170×10^{-4} cm^{-1}) are reasonable for a square-pyramidal Cu^{II} with four N atoms in the basal plane and axial elongation. The fit in the perpendicular

dx.doi.org/10.1021/ic302499f | *Inorg. Chem.* 2013, 52, 3084−3093

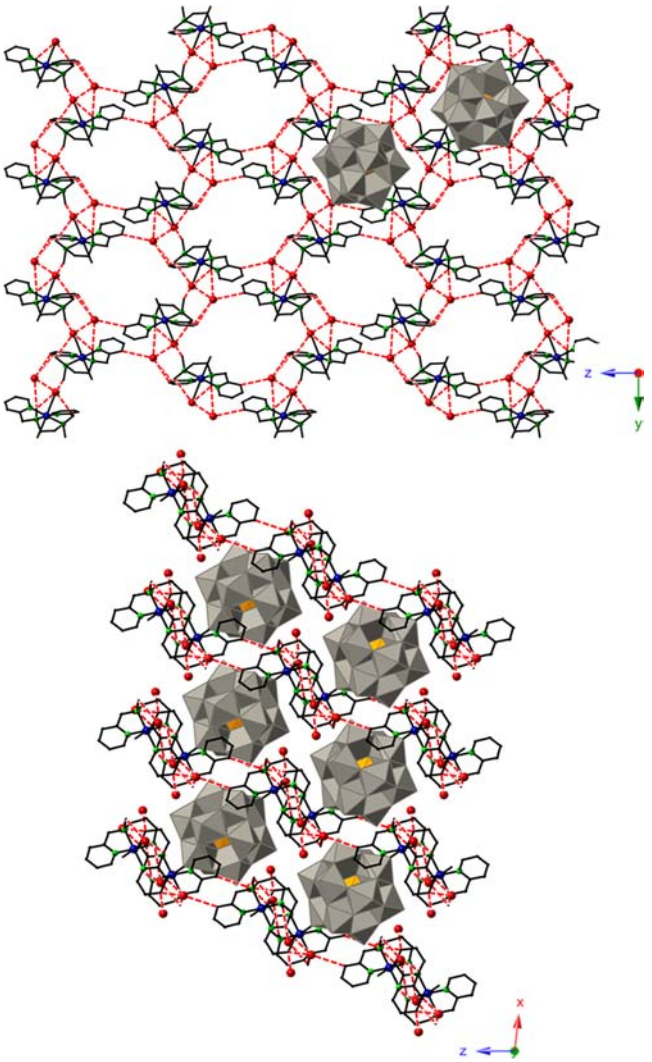

Figure 8. Top: Projection of a metal−organic honeycomb-like layer of **2** on the *bc* plane with a detail of two adjacent Keggin clusters (C−H···O_w hydrogen bonds: red dashed lines). Bottom: Crystal packing of **2** viewed along the *b* axis.

region requires the introduction of rhombic symmetry in **g** and **A** tensors (Table S5 in the Supporting Information), most likely because the values of their components are slightly different for each Cu^{II}.

The Q-band spectrum of the anhydrous **1a** is upfield shifted compared to that of **1**. This shift and consequent smaller *g* values are consistent with the elongation of the apical Cu−O bonds observed by X-ray diffraction for both Cu1A and Cu1B upon dehydration (Table 3). The hyperfine structure on the parallel region is maintained in **1a**, but the spacing between the four lines becomes irregular. This could be explained on the basis of a more pronounced elongation for one of the Cu^{II} atoms, which would lead to differences in the coordination geometries significant enough for the EPR signals to start differentiating in the parallel region. This is in agreement with structural data, which shows that while apical elongation of Cu1A is ∼0.1 Å, release of the water molecule for Cu1B and consequent coordination to a POM results in a considerably larger lengthening of the Cu1B−O_{ap} bond (∼0.5 Å). Simulation of the spectrum with axial symmetry affords the *g* and *A* values displayed in Table S5 in the Supporting

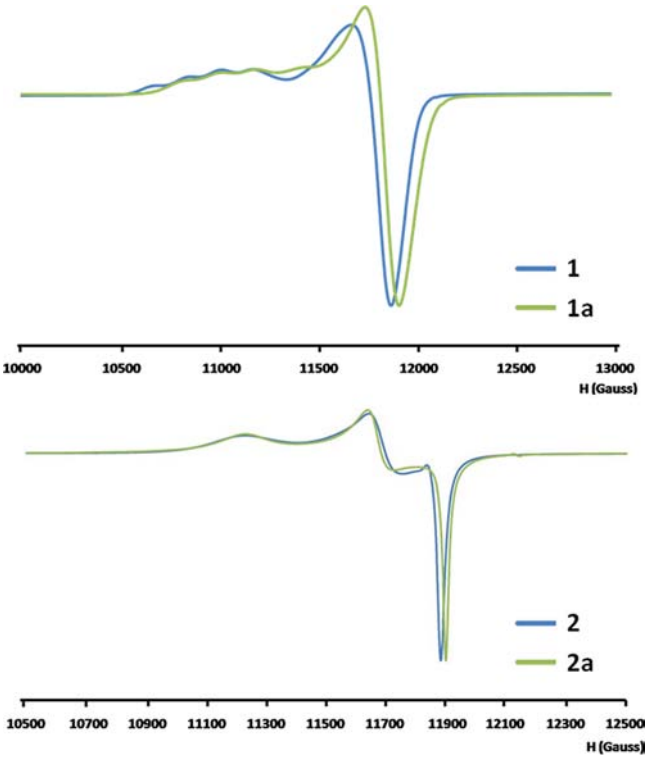

Figure 9. Comparison between the room-temperature Q-band EPR spectra of compounds **1** and **1a** (top) and **2** and **2a** (bottom).

Information for the two averaged Cu^{II} atoms. However, if $A_{\|}$ is considered constant (170×10^{-4} cm^{-1}) and the first and fourth lines on the parallel region are assigned to different Cu^{II} atoms, the fit results in different $g_{\|}$ values for each atom (2.195 and 2.175). Taking into account the Cu−O_{ap} bond lengths, the latter $g_{\|}$ values appear to better describe our system.

Considering the similarities of the Cu^{II} chromophores in compounds **1** and **2** (both with axial geometries, four N atoms of almost identical ligands in the equatorial/basal plane, O_w or O_{POM} atoms in axial/apical positions, comparable Cu−N/Cu−O bond lengths and angles), an EPR signal of axial symmetry should also be a priori expected for **2** in close analogy to the experimental observations in **1**. However, the EPR spectrum of **2** (Figure 9, bottom) shows clear rhombic symmetry, and furthermore, the hyperfine structure in this rhombic signal is collapsed. A narrower, still collapsed rhombic signal was observed at higher field for **2a**. The **g** tensors originating these rhombic signals appear to be cooperative tensors associated to a certain phenomenon operating in our Cu^{II} system rather than molecular tensors describing the individual geometries of our $Cu^{II}N_4O_2$ (**2**) or $Cu^{II}N_4O$ (**2a**) chromophores. This is supported by the fact that the calculated *g* values (Table S5 in the Supporting Information) do not undergo significant variation with the change from the octahedral $Cu^{II}N_4O_2$ to square-pyramidal $Cu^{II}N_4O$ chromophore and consequent shortening of the Cu−O_{ap} bond (Table 3), observed upon dehydration. Fluxional behavior originating from a dynamic Jahn−Teller effect or the presence of long-range magnetic interactions appears to be the most plausible among all phenomena that could lead to a rhombic signal with collapsed hyperfine structure associated to a Cu^{II} system like ours. The low g_1 values obtained for both **2** and **2a** would be in agreement with this type of fluxional behavior, which should be reflected in a shift of the spectrum with decreasing temperature. However,

dx.doi.org/10.1021/ic302499f | *Inorg. Chem.* 2013, 52, 3084−3093

no significant change takes place at low temperatures (Figure S12 in the Supporting Information); hence any dynamic Jahn–Teller effect can be ruled out. Therefore, we believe that our spectra can be attributed to **g** being an exchange cooperative tensor ($G = 2.59$)[24] instead of a molecular one, and therefore, that long-range, extremely weak magnetic interactions are present in both **2** and **2a**. It is known that rhombic signals are obtained when cooperative **g** tensors refer to interacting Cu^{II} polyhedra with different orientations in the unit cell.[25] Moreover, long-range, weak magnetic interactions between distant Cu^{II} atoms have been found to have a clear effect in the EPR spectra. For example, this is the case of $[Cu(py)_2Cl_2]$, where Cu^{II} atoms separated by ca. 9 Å and connected by sequences of six consecutive bonds and interactions were found to be coupled on the basis of EPR spectroscopy.[26]

CONCLUSIONS

Two new hybrid compounds based on Keggin anions and Cu^{II} complexes of N_2Py_2 tetradentate ligands have been hydrothermally prepared, $[Cu(bpmen)(H_2O)][SiW_{12}O_{40}\{Cu(bpmen)\}]$ (**1**) and $[SiW_{12}O_{40}\{Cu(bpmpn)(H_2O)\}_2]\cdot 3H_2O$ (**2**) (bpmen, N,N′-dimethyl-N,N′-bis-(pyridin-2-ylmethyl)-1,2-diaminoethane; bpmpn, N,N′-dimethyl-N,N′-bis(pyridin-2-ylmethyl)-1,3-diaminopropane). The structure of **1** shows complex cations enclosed between rows of monodecorated POMs, whereas the *trans*-didecorated species of **2** forms stacked honeycomb-like metal–organic layers with Keggin clusters accommodated in channels. Structural differences relate to changes in the complex geometry (square-pyramidal vs. octahedral) and ligand conformation (*cis vs. trans*) when going from bpmen to bpmpn.

This work represents a nice example of how functionalization of POMs with transition metal complexes can endow the POM system with interesting features. In our case, the choice of Cu^{II}/N_2Py_2 moieties has resulted in two hybrid compounds showing structural response to thermal stimuli regardless of the exact nature of the ligand. Both compounds undergo single-crystal to single-crystal transformations promoted by dehydration processes that have been followed by powder and single-crystal X-ray diffraction, allowing for the structures of the high-temperature, anhydrous phases **1a** and **2a** to be determined. Dehydration and consequent structural transformations are fully reversible without collapse of the crystallinity despite the fact that they involve variations in the Cu^{II}–O bonding, coordination geometries, and ligand conformation. Release of the apical water molecule from the complex cation, followed by coordination to a contiguous POM, leads to the formation of *cis*-didecorated neutral species in **1a**, whereas the packing of **2a** is maintained owing to a new network of $C-H\cdots O_{POM}$ interactions arising from overall compression. The effect of these structural changes is reflected in the EPR spectra.

ASSOCIATED CONTENT

Supporting Information

^1H NMR spectra (Figure S1) and synthetic scheme (Figure S3) for bpmen and bpmpn; PXRD diffractograms of **2**, other precipitates, and TGA residues (Figures S2 and S7); IR and Raman spectra (Figures S4 and S5); TGA/DTA curves (Figure S6); Cu^{II}/N_2Py_2 isomers (Figure S8); POM-aromatic interactions in **1**/**1a** (Figure S9); additional structural figures for **2**/**2a** (Figures S10 and S11); X-band EPR spectra of **2**/**2a** (Figures S12 and S14) and **1**/**1a** (Figure S13); ranges of W–O bond lengths (Table S1); selected bond lengths and angles for Cu^{II}/N_2Py_2 complexes (Table S2); C–H···O interactions for **1**/**1a** and **2**/**2a** (Tables S3 and S4); and spin Hamiltonian parameters (Table S5). Crystallographic data in CIF format for **1**, **2**, **1a**, **2a**, and rehydrated **1**. This material is available free of charge via the Internet at http://pubs.acs.org.

AUTHOR INFORMATION

Corresponding Author

*E-mail: juanma.zorrilla@ehu.es.

Funding

Eusko Jaurlaritza/Gobierno Vasco (EJ/GV) and Universidad del País Vasco UPV/EHU.

Notes

The authors declare no competing financial interest.

ACKNOWLEDGMENTS

This work has been funded by EJ/GV through the Program to Support the Research Groups of the Basque University System (grant IT477-10) and the SAIOTEK Program (grant S-PE11UN062). The authors thank UPV/EHU for financial support (grant UFI11/53). A.I. and B.A. are indebted to EJ/GV for their predoctoral fellowships. Technical and human support provided by SGIker (UPV/EHU) is gratefully acknowledged.

REFERENCES

(1) (a) Pope, M. T. *Heteropoly and Isopoly Oxometalates*; Springer: Berlin, Germany, 1983. (b) Hill, C. L. *Chem. Rev.* **1998**, *98* (1), thematic issue. (c) *Polyoxometalates: From Platonic Solids to Anti-Retroviral Activity*; Pope, M. T., Müller, A., Eds.; Kluwer: Dordrecht, The Netherlands, 1994. (d) *Polyoxometalate Chemistry: From Topology via Self-Assembly to Applications*; Pope, M. T., Müller, A., Eds.; Kluwer: Dordrecht, The Netherlands, 2001. (e) *Polyoxometalate Chemistry for Nano-Composite Design*; Yamase, T., Pope, M. T., Eds.; Kluwer: New York, 2002. (f) Kortz, U., Ed. *Eur. J. Inorg. Chem.* **2009**, *2009* (34), thematic issue. (g) Long, D.-L.; Cronin, L. *Dalton Trans.* **2012**, *33* (41), thematic issue. (h) Cronin, L.; Müller, A., Eds. *Chem. Soc. Rev.* **2012**, *41* (22), thematic issue.

(2) Dolbecq, A.; Dumas, E.; Mayer, C. R.; Mialane, P. *Chem. Rev.* **2010**, *110*, 6009.

(3) (a) Gómez-Romero, P. *Adv. Mater.* **2001**, *13*, 163. (b) Long, D.-L.; Tsunashima, R.; Cronin, L. *Angew. Chem., Int. Ed.* **2010**, *49*, 1736.

(4) (a) Cao, R.; Liu, S.; Cao, J.; Wang, L.; Tang, Q.; Liu, Y.; Ren, Y. *J. Mol. Struct.* **2008**, *888*, 307. (b) Chubarova, E. V.; Klöck, C.; Dickman, M. H.; Kortz, U. *J. Cluster Sci.* **2007**, *18*, 697. (c) Klistincová, L.; Rakovský, E.; Schwendt, P. *Inorg. Chem. Commun.* **2008**, *11*, 1140. (d) Wang, T.; Peng, J.; Liu, H.; Zhu, D.; Tian, A.; Wang, L. *J. Mol. Struct.* **2008**, *892*, 268. (e) An, H.; Xu, T.; Wang, E.; Meng, C. *Inorg. Chem. Commun.* **2007**, *10*, 1453. (f) An, H.-Y.; Wang, E.-B.; Xiao, D.-R.; Li, Y.-G.; Su, Z.-M.; Xu, L. *Angew. Chem., Int. Ed.* **2006**, *45*, 904.

(5) See, for example: (a) Henkel, G.; Krebs, B. *Chem. Rev.* **2004**, *104*, 801. (b) Kim, E.; Chufán, E. E.; Kamaraj, K.; Karlin, K. D. *Chem. Rev.* **2004**, *104*, 1077. (c) Nakamura, E.; Mori, S. *Angew. Chem., Int. Ed.* **2000**, *39*, 3750. (d) Thomas, A. W.; Ley, S. V. *Angew. Chem., Int. Ed.* **2003**, *42*, 5400. (e) Beletskaya, I. P.; Cheprakov, A. V. *Coord. Chem. Rev.* **2004**, *248*, 2337. (f) Pintauer, T.; Matyjaszewski, K. *Coord. Chem. Rev.* **2005**, *249*, 1155.

(6) (a) Reinoso, S.; Vitoria, P.; Lezama, L.; Luque, A.; Gutiérrez-Zorrilla, J. M. *Inorg. Chem.* **2003**, *42*, 3709. (b) San Felices, L.; Vitoria, P.; Gutiérrez-Zorrilla, J. M.; Reinoso, S.; Etxebarria, J.; Lezama, L. *Chem.—Eur. J.* **2004**, *10*, 5138. (c) Reinoso, S.; Vitoria, P.; San Felices, L.; Lezama, L.; Gutiérrez-Zorrilla, J. M. *Chem.—Eur. J.* **2005**, *11*, 1538. (d) Reinoso, S.; Vitoria, P.; Gutiérrez-Zorrilla, J. M.; Lezama, L.; San Felices, L.; Beitia, J. I. *Inorg. Chem.* **2005**, *44*, 9731. (e) Reinoso, S.; Vitoria, P.; San Felices, L.; Lezama, L.; Gutiérrez-Zorrilla, J. M. *Inorg. Chem.* **2006**, *45*, 108. (f) Reinoso, S.; Vitoria, P.; Gutiérrez-Zorrilla, J. M.; Lezama, L.; Madariaga, J. M.; San Felices, L.; Iturrospe, A. *Inorg.*

Chem. **2007**, *46*, 4010. (g) Reinoso, S.; Vitoria, P.; San Felices, L.; Montero, A.; Lezama, L.; Gutiérrez-Zorrilla, J. M. *Inorg. Chem.* **2007**, *46*, 1297.
(7) (a) Costas, M.; Mehn, M. P.; Jensen, M. P.; Que, L. *Chem. Rev.* **2004**, *104*, 939. (b) Zhang, J.; Zheng, H.; Groce, S. L.; Lipscomb, J. D. *J. Mol. Catal. A* **2006**, *251*, 54. (c) Groni, S.; Blain, G.; Guillot, R.; Policar, C.; Anxolabéhére-Mallart, E. *Inorg. Chem.* **2007**, *46*, 1951. (d) Martinho, M.; Banse, F.; Sainton, J.; Philouze, C.; Guillot, R.; Blain, G.; Dorlet, P.; Lecomte, S.; Girerd, J. J. *Inorg. Chem.* **2007**, *46*, 1709.
(8) Glerup, J.; Hazell, A.; Michelsen, K. *Acta Chem. Scand.* **1991**, *45*, 1025.
(9) Tezé, A.; Hervé, G.; Finke, R. G.; Lyon, D. K. *Inorganic Syntheses*; Ginsberg, P. A., Ed.; John Wiley & Sons: Hoboken, NJ, 1990; Vol. *27*, pp 85−96.
(10) White, M. C.; Doyle, A. G.; Jacobsen, E. N. *J. Am. Chem. Soc.* **2001**, *123*, 7194.
(11) *CrysAlisPro Software System*; Agilent Technologies UK Ltd.: Oxford, U. K., 2012.
(12) Dolomanov, O. V.; Bourhis, L. J.; Gildea, R. J.; Howard, J. A. K.; Puschmann, H. *J. Appl. Crystallogr.* **2009**, *42*, 339.
(13) Sheldrick, G. M. *Acta Crystallogr.* **2008**, *A64*, 112.
(14) Macrae, C. F.; Bruno, I. J.; Chisholm, J. A.; Edgington, P. R.; McCabe, P.; Pidcock, E.; Rodriguez-Monge, L.; Taylor, R.; van de Streek, J.; Wood, P. A. *J. Appl. Crystallogr.* **2008**, *41*, 466.
(15) Spek, A. L. *Acta Crystallogr.* **2009**, *D65*, 148.
(16) Farrugia, L. J. *J. Appl. Crystallogr.* **1999**, *32*, 837.
(17) Rocchiccioli-Deltcheff, C.; Fournier, M.; Franck, R.; Thouvenot, R. *Inorg. Chem.* **1983**, *22*, 207 and references therein.
(18) (a) Bridgeman, A. J. *Chem. Phys.* **2003**, *287*, 55. (b) San Felices, L.; Vitoria, P.; Gutiérrez-Zorrilla, J. M.; Lezama, L.; Reinoso, S. *Inorg. Chem.* **2006**, *45*, 7748.
(19) Schofield, P. F.; Knight, K. S.; Redfern, S. A. T.; Cressey, G. *Acta Crystallogr.* **1997**, *B53*, 102.
(20) Woodward, P. M.; Sleight, A. W.; Vogt, T. *J. Phys. Chem. Solids* **1995**, *56*, 1305.
(21) (a) Kani, Y.; Ohba, S.; Kunita, M.; Nishida, Y. *Acta Crystallogr.* **2000**, *C56*, e197. (b) Mautner, F. A.; Mikuriya, M.; Ishida, H.; Sakiyama, H.; Louka, F. R.; Humphrey, J. W.; Massoud, S. S. *Inorg. Chim. Acta* **2009**, *362*, 4073. (c) Glerup, J.; Goodson, P. A.; Hodyson, D. J.; Michelson, K. *Inorg. Chem.* **1995**, *34*, 6255. (d) Pandiyan, T.; Guadalupe, H. J.; Cruz, J.; Bernès, S.; Ugalde-Saldivar, V. M.; González, I. *Eur. J. Inorg. Chem.* **2008**, 3274. (e) Xu, H.; Sato, O.; Li, Z.; Ma, J. *Inorg. Chem. Commun.* **2012**, *15*, 311.
(22) Yokoyama, T.; Yoshise, M.; Hase, S.; Kawate, A.; Akashi, H.; Zenki, M. *X-Ray Struct. Anal. Online* **2011**, *27*, 51.
(23) Ugalde, M.; Gutiérrez-Zorrilla, J. M.; Vitoria, P.; Luque, A.; Wéry, A. S. J.; Román, P. *Chem. Mater.* **1997**, *9*, 2869.
(24) Hathaway, B. J.; Billing, D. *Coord. Chem. Rev.* **1970**, *5*, 143.
(25) See, for example: (a) Henke, W.; Kremer, S.; Reinen, D. *Inorg. Chem.* **1983**, *22*, 2858. (b) Cortés, R.; Lezama, L.; Larramendi, J. I. R.; Insausti, M.; Folgado, J. V.; Madariaga, G.; Rojo, T. *J. Chem. Soc., Dalton Trans.* **1994**, 2573. (c) Caballero, A. B.; Rodríguez-Diéguez, A.; Lezama, L.; Barea, E.; Salas, J. M. *Dalton Trans.* **2011**, *40*, 5180.
(26) Hughes, R. C.; Morosin, B.; Richards, P. M. *Phys. Rev. B* **1975**, *11*, 1795.